

# Infrared Absorption Enhancement for CO Adsorbed on Au Films in Perchloric Acid Solutions and Effects of Surface Structure Studied by Cyclic Voltammetry, Scanning Tunneling Microscopy, and Surface-Enhanced IR Spectroscopy

Shi-Gang Sun,<sup>\*,†</sup> Wen-Bin Cai,<sup>‡</sup> Li-Jun Wan,<sup>‡</sup> and Masatoshi Osawa<sup>\*,‡</sup>

Catalysis Research Center, Hokkaido University, Sapporo 060, Japan, and State Key Laboratory for Physical Chemistry of Solid Surfaces, Department of Chemistry, Institute of Physical Chemistry, Xiamen University, Xiamen 361005, China

Received: October 12, 1998; In Final Form: January 20, 1999

The adsorption of CO on Au thin film electrodes vacuum-deposited on silicon substrate has been studied in 0.1 M perchloric acid solution by surface-enhanced infrared absorption spectroscopy (SEIRAS) with the Kretschmann attenuated-total-reflection configuration. Scanning tunneling microscopy (STM) was used to investigate the surface structures of the Au films subjected to different treatments. The IR absorption of CO adsorbed on the Au film electrodes is 20 times larger than that of CO adsorbed on bulk Au electrodes measured by reflection–absorption spectroscopy. When the Au film is subjected to flame annealing, which reorients the crystallites of the Au film and results in a highly ordered (111) surface, the enhancement factor is increased further to ca. 40. Cyclic voltammetric studies demonstrated that the highly ordered Au(111) films possess a higher electrocatalytic activity toward CO oxidation than polycrystalline Au films without flame annealing. Two different linearly bonded CO species,  $\text{CO}_\text{L}$  and  $\text{CO}_\text{L}(\text{s})$ , were identified on the polycrystal Au surface without flame annealing. The  $\text{CO}_\text{L}$  is the predominant adsorbate that yields the IR absorption at 2110–2136  $\text{cm}^{-1}$ . The  $\text{CO}_\text{L}(\text{s})$  species is a minor adsorbate and gives rise to the IR absorption at 2020–2045  $\text{cm}^{-1}$ , which is assigned to CO adsorbed at specific surface sites located at boundaries of Au crystallites and very close to the surface of the silicon substrate. On the highly ordered Au(111) surface prepared by flame annealing, an additional weak band assigned to bridge-bonded CO species ( $\text{CO}_\text{B}$ ) was detected at 1925–1975  $\text{cm}^{-1}$  in a narrow potential range (0.0–0.4 V vs SCE). The present study puts emphasis on effects of surface structures of Au films for IR absorption enhancement and demonstrates also that the Au films prepared by vacuum evaporation is of great importance in fundamental studies as well as in electrocatalysis applications.

## Introduction

The adsorption and oxidation of carbon monoxide (CO) on metal electrodes is an active field of electrochemistry and electrocatalysis and has been studied extensively.<sup>1–3</sup> Among numerous techniques employed in the study of CO adsorption and oxidation, in situ infrared reflection–absorption spectroscopy (IRAS) presents advantages in investigating the coordination of CO to surfaces of metals, especially of transition metals belonging to group VIII of the periodical table. The adsorption and oxidation of CO on smooth surfaces of both poly- and single-crystal electrodes (Pt, Pd, Rh, and Ir) have been studied extensively by IRAS in the past.<sup>4–12</sup> Gold, which differs from the transition metals by its electronic configuration of fully occupied d-orbitals ( $5\text{d}^{10}6\text{s}^1$ ), exhibits a weaker coordination ability for CO but performs as a good electrocatalyst for CO oxidation in both acid and alkaline solutions.<sup>13,14</sup> Previous IRAS and surface-enhanced Raman scattering (SERS) studies on the CO adsorption on poly- and single-crystal Au electrodes demonstrated that the adsorption of CO from acid solution is very weak.<sup>4,15–20</sup> Weak IR and Raman bands assigned to linearly bonded CO ( $\text{CO}_\text{L}$ ) have been observed above 2100  $\text{cm}^{-1}$ . The IR absorption of bridge-bonded CO ( $\text{CO}_\text{B}$ ) has been observed only on the Au(210) electrode at around 1950  $\text{cm}^{-1}$ .<sup>20</sup> In alkaline

solutions the adsorption of CO is much stronger and gives a strong IR band at around 1950  $\text{cm}^{-1}$ , which has been ascribed to a bridge coordination to gold surface.

The use of thin metal films supported on a conductive substrate is a convenient way to prepare electrocatalysts with high activity at low costs. The deposition of metal nanoparticles and adsorption of metal atoms on different substances have been studied extensively.<sup>21–25</sup> Such approaches have become a very active field of electrochemical studies. For the fabrication of active catalysts and for full control of catalytic reactions, detailed analyses of the thin metal films (surface structures and chemical nature) are required. Since the vibrational frequency of CO is sensitive to the adsorption sites, this molecule is useful as a probe to characterize metal electrode surfaces.

Thin metal films consisting of fine particles (island films) exhibit interesting optical properties. It has been revealed that molecules adsorbed on Au and Ag films supported on IR transparent substrates induce enhanced IR absorption, with the enhancement factor ranging from 1 to 2 orders of magnitude.<sup>26–30</sup> This phenomenon was named surface-enhanced IR absorption (SEIRA) by analogy to SERS. SEIRA has been successfully applied to studies of electrochemical interfaces by Osawa and co-workers.<sup>31–35</sup> Recently, Sun and his group have revealed the abnormal infrared effects (AIREs) on continuous transition metal films with nanometer thickness grown on conductive substrates (typically on glassy carbon substrate).<sup>23,36,37</sup> They found that,

\* Corresponding author.

<sup>†</sup> Xiamen University.

<sup>‡</sup> Hokkaido University.

in addition to the enhancement of IR absorption, CO and other molecules adsorbed on thin film electrodes of transition metals exhibit "negative" absorption (that is, the inversion of the sign of peaks). In both SEIRA and AIREs, the control of the thickness and the structure of the films is important for the IR absorption enhancement. Osawa et al. have theoretically suggested that vibrational modes of adsorbates on thin metal films yield either positive (i.e., normal) or negative (i.e., inverse) absorption depending on the structure of the film and optical properties of the substrate.<sup>29</sup> The study of effects of surface structures of thin films on IR absorption enhancement will contribute to the understanding of essential aspects behind the SEIRA and AIREs.

From the viewpoints described above, IR studies of the CO adsorption on thin metal film electrodes are interesting and important in electrochemistry and surface spectroscopy. In the present paper, the adsorption of CO on Au films with different structures supported on silicon has been studied by cyclic voltammetry, scanning tunneling microscopy (STM), and SEIRA spectroscopy (SEIRAS). The effects of surface structures of the Au films on IR absorption enhancement and electrocatalysis will be discussed.

### Experimental Section

A 20 nm thick Au film was formed by evaporation of Au onto the base plane of a silicon hemicylindrical prism (1 cm in radius and 2.5 cm in height) at a pressure of  $5 \times 10^{-5}$  Pa. The deposition rate of Au on the silicon substrate was controlled to  $0.01 \text{ nm s}^{-1}$  with a quartz microbalance built inside the vacuum evaporation chamber. The Au film and the silicon prism served as the working electrode and IR window, respectively, for *in situ* SEIRAS measurements. For the purpose of obtaining an ordered surface, the Au film was annealed using a hydrogen-oxygen flame and cooled subsequently in an air atmosphere. The apparent electrode area of Au film was defined physically by an O-ring of 1.45 cm i.d. that limits the electrolyte solution from making contact with other parts of the Au film and yields a geometric area of  $1.65 \text{ cm}^2$ .

The cyclic voltammetric studies were carried out with an HAB-151 potentiostat/galvanostat (Hokuto Ltd.), and the potential sweep rate was fixed at  $50 \text{ mV s}^{-1}$ . A Nanoscope E scanning tunneling microscope (Digital Instruments) was employed for the *ex situ* structural analysis of evaporated Au films subjected to different treatments.

*In situ* SEIRAS studies were performed with a FTS 575C Fourier transform infrared spectrometer (Bio-Rad) with the so-called Kretschmann attenuated-total-reflection (ATR) configuration (an ATR measurements using a prism/thin metal film/solution geometry).<sup>31–35</sup> The infrared radiation from a light source was passed into the silicon window with an incident angle of  $60^\circ$  and reflected at the electrode/solution interface.

To study the potential dependence of CO adsorption on evaporated Au films and to compare our results with previous IRAS studies of CO adsorption on poly- or single-crystal Au electrodes, the multistep FTIRS procedure<sup>10</sup> was used in the present study. In this procedure a series of single-beam spectra were collected stepwise at sample potentials ( $E_s$ ) where the adsorbed CO is stable, and a single-beam spectrum was collected finally at reference potential ( $E_r$ ) at which the adsorbed CO has been removed completely by electrooxidation. The resulting spectra were calculated according to following formula

$$\frac{\Delta R}{R} = \frac{R(E_r) - R(E_s)}{R(E_r)} \quad (1)$$

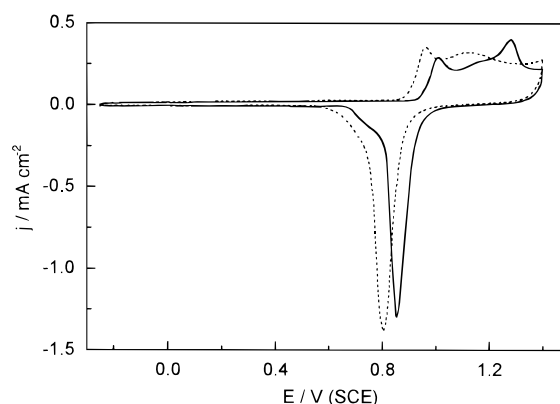


**Figure 1.** Cyclic voltammograms of Au film electrodes before (dashed curve) and after flame treatment (solid curve) in 0.1 M  $\text{HClO}_4$ . Sweep rate was  $50 \text{ mV s}^{-1}$ .

where  $\Delta R/R$  represents the relative change in reflectivity and  $R(E_r)$  and  $R(E_s)$  are single-beam spectra collected at reference and sample potentials, respectively. With this definition, the IR absorption of surface CO at  $E_s$  will yield positive-going bands in the resulting spectra. The spectral resolution was at  $4 \text{ cm}^{-1}$ , and 256 interferograms were scanned and co-added into each single-beam spectrum.

Solutions (0.1 M  $\text{HClO}_4$ ) were prepared from Millipore water and super pure perchloric acid (Cica-Merck, Kanto Chemical Co., Inc.). Before each measurement the solution was deaerated by bubbling pure Ar gas. In the process of CO adsorption, the solution was saturated with CO by continuously bubbling CO gas of high purity (99.5%, Hokusan Co.). The reference electrode used in cyclic voltammetry and SEIRAS studies was a saturated calomel electrode (SCE), and potentials reported in the present paper were quoted versus this SCE. All experiments were carried out at room temperature ( $\sim 20^\circ \text{C}$ ).

### Results and Discussion

**1. Cyclic Voltammetry and STM Characterizations of Surface Structure of Evaporated Au Films before and after Flame Annealing.** As shown in Figure 1, the stable cyclic voltammogram (CV) recorded on an Au film electrode as evaporated on a silicon substrate and subjected to potential cycling (denoted thereafter as Au(a)) exhibits CV features (dashed trace) similar to those of polycrystalline Au electrodes. Oxidation of the electrode surface in the positive-going potential sweep (PGPS) yields a sharp current peak around 0.96 V followed by a broad peak near 1.12 V. The reduction of the oxidized Au surface is characterized by a large negative current peak close to 0.80 V in the negative-going potential sweep (NGPS). When the Au film was subjected to flame annealing, the most significant change of CV features consists of the appearance of a sharp current peak of surface oxidation near 1.01 V (solid trace). The voltammogram recorded on the Au film electrode after flame annealing (denoting thereafter as Au(b)) is very similar to that of a gold single-crystal electrode with (111) orientation in the same perchloric acid solution.<sup>38–40</sup> This result indicates primarily that after flame annealing the Au surface may become highly ordered toward (111) orientation. It is interesting to note that both the current peaks of oxidation and reduction of the Au(b) electrode were shifted positively by about 50 mV in comparison with the data measured on the Au(a) electrode, implying that the Au film after flame annealing manifests a slightly higher resistance to surface oxidation–reduction processes.

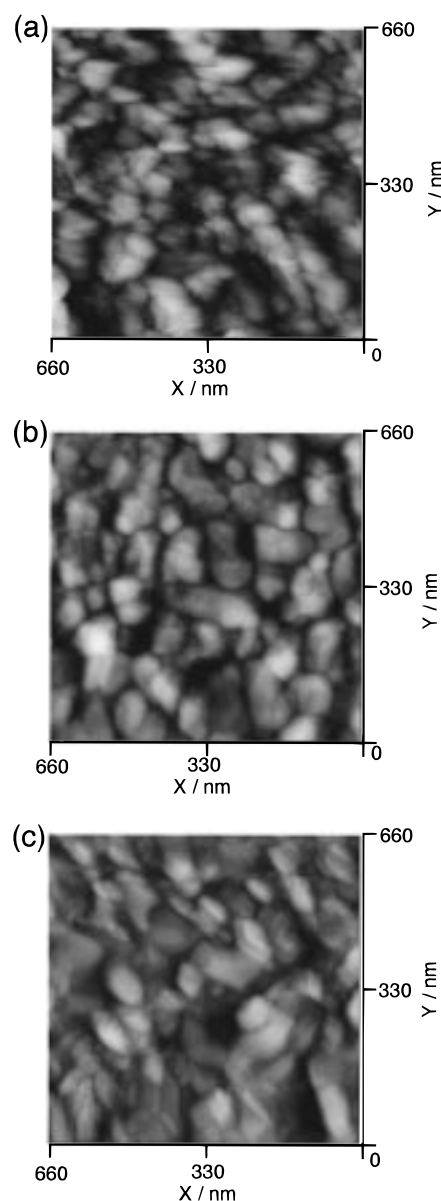
The electric charge of oxygen adsorption ( $Q_{\text{ad}}^{\text{O}}$ ) in the PGPS and the charge of oxide reduction ( $Q_{\text{re}}^{\text{O}}$ ) in the NGPS can be measured by integrating the voltammograms in Figure 1. The values of  $Q_{\text{ad}}^{\text{O}}$  are measured at 2.70 and 2.27 mC, respectively, for electrodes of Au(a) and Au(b), and the associated values of  $Q_{\text{re}}^{\text{O}}$  are 2.73 and 2.24 mC. The difference between  $Q_{\text{ad}}^{\text{O}}$  and  $Q_{\text{re}}^{\text{O}}$  for both electrodes is estimated to be about 1%; such a small deviation may imply that the surface oxide formed in the PGPS has been reduced completely in the NGPS and that no oxygen evolution occurs in the PGPS under the present upper limit of potential cycling. The reduction charge  $Q_{\text{re}}^{\text{O}}$  was used to estimate the active area and roughness factor of the Au film electrode by taking the theoretical value of  $0.44 \text{ mC cm}^{-2}$  for a monolayer of oxygen species on an Au(111) electrode<sup>39,40</sup> in the calculation. The active area of the Au(a) electrode is calculated to be  $6.20 \text{ cm}^2$  (roughness factor of 3.75) and that of the Au(b) electrode is measured to be  $5.09 \text{ cm}^2$  (roughness factor of 3.07). The decrease in surface roughness indicates that the Au film may become more compact by flame annealing.

Figure 2 is a set of scanning tunneling microscopy (STM) images of evaporated Au films on silicone subjected to different treatments. The measurements were carried out in air with the current mode. The Au film without any treatment shown in Figure 2a consists of crystallites of irregular round shape with an average size of ca. 60 nm. The Au film subjected to potential cycling between  $-0.25$  and  $1.40 \text{ V}$  appears in a different morphology as shown in Figure 2b. It can be seen that the boundaries between crystallites become more distinct, which may imply the dissolution of impurities adsorbed on the surface during the evaporation process. Furthermore, the crystals are slightly larger and exhibit a rectangular shape. The average length and width of the crystallites are measured to be ca. 105 and 52 nm, respectively. A dramatic morphological change takes place by flame annealing of the Au film, as is seen from the STM image displayed in Figure 2c. All crystallites are oriented preferentially, though the size of the crystallites remains almost unchanged.

To illustrate the surface structure of the flame-annealed Au film more clearly, STM images observed in the height mode are shown in Figure 3. Image a in the figure (scan area of  $660 \times 660 \text{ nm}^2$ ) clearly shows that the crystallites exhibit hexagonal patterns on top, indicating an fcc (111) symmetry. The average size of the hexagonal patterns of crystallites was ca.  $88 \text{ nm} \times 59 \text{ nm}$ . Image b ( $100 \times 100 \text{ nm}^2$ ) is an expanded one of a crystallite located near the center on image a, which shows that the surface of the crystallite consists of flat terraces and steps. The height of the steps was measured to be  $0.24 \text{ nm}$  (monatomic height). If we observe the terraces with atomic resolution, the hexagonal arrangement of surface atoms characteristic of a Au-(111)-(1  $\times$  1) surface is as shown in Figure 3c. The STM observation is consistent with the change in the cyclic voltammetric behavior by flame annealing.

Haiss and co-workers<sup>41</sup> and Batina et al.<sup>42,43</sup> have reported that thick ( $\sim 200 \text{ nm}$ ) Au films evaporated on glasses and annealed at  $1000^\circ\text{C}$  produced compact "continuous" films with large atomically flat (111) terraces. One may think that such continuous films are more favorable for electrochemistry than our island (or discontinuous) films. However, it is noted that the island nature of the metal films facilitates the excitations of plasmon modes of the metal, resulting in SEIRA.<sup>28–31,35</sup> The following sections will concentrate on the adsorption of CO on the thin Au film electrodes with different structures.

## 2. Cyclic Voltammetric Studies of CO Adsorption on Au Film Electrodes with Different Surface Structures. Cyclic



**Figure 2.** STM images ( $660 \text{ nm} \times 660 \text{ nm}$ ) of an Au film evaporated on Si substrate subjected to different treatments: (a) as evaporated; (b) after potential cycling between  $-0.25$  and  $1.40 \text{ V}$ ; (c) after flame annealing. All the images were obtained in the current mode.

voltammograms for CO adsorption and oxidation on Au film electrodes with and without flame annealing, Au(a) and Au(b) electrodes, are shown in Figure 4, which were recorded in  $0.1 \text{ M HClO}_4$  solution saturated with CO after holding the potential at  $0.0 \text{ V}$ . In the case of the Au(a) electrode (dashed trace), a large oxidation peak appears around  $0.34 \text{ V}$  in the PGPS, which is ascribed mainly to the oxidation of adsorbed CO species that was formed at  $0.0 \text{ V}$  before starting the potential scan. Following the increase of the potential in the PGPS, the current peaks for surface oxidation of the Au film electrode is observed. We can see that the oxidation current of Au is superimposed on the oxidation current of the solution CO species and remains the same character seen in Figure 1. When the electrode potential is decreased from  $1.40$  to  $1.0 \text{ V}$  in the NGPS, the current decreases to almost zero, indicating that the solution CO species cannot be oxidized under the present conditions. This is due to the inhibition of CO oxidation by a surface Au oxide formed at potentials above  $1.0 \text{ V}$  in the PGPS.<sup>44,45</sup> Following the decrease of the electrode potential in the NGPS, an oxidation current



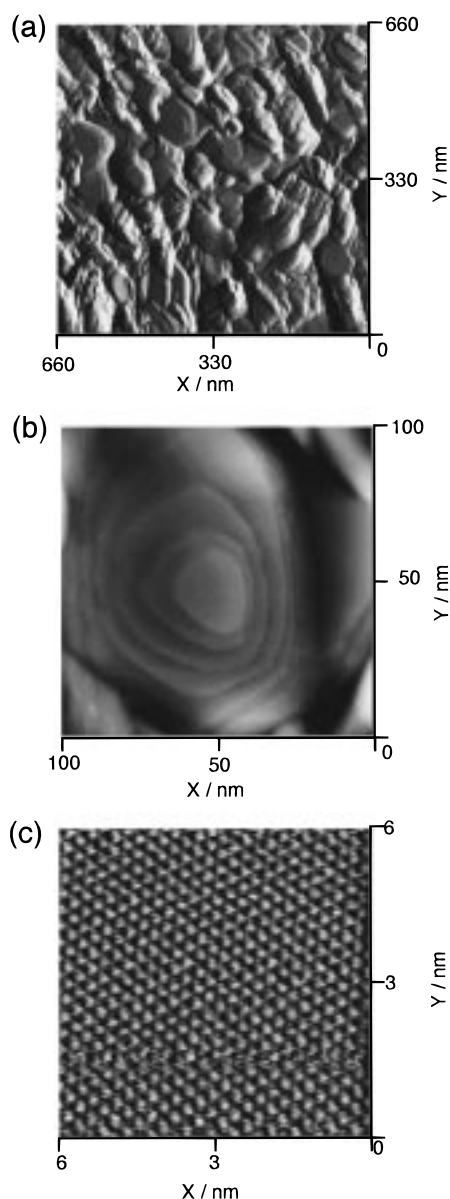


**Figure 3.** STM images of a flame-annealed Au film: (a) height mode presentation of Figure 2c; (b) expanded (100 nm  $\times$  100 nm) image of a particle in image a; (c) further expanded (6 nm  $\times$  6 nm) image of the terrace in image b, showing the arrangement of surface Au atoms.

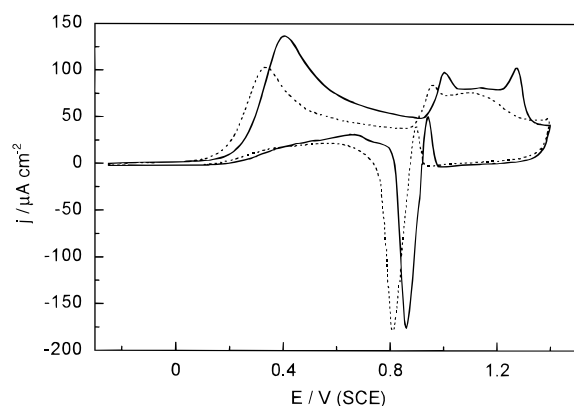


**Figure 4.** Cyclic voltammograms of an Au film before (dashed curve) and after flame treatment (solid curves) recorded in CO-saturated 0.1 M HClO<sub>4</sub>. Sweep rate was 50 mV s<sup>-1</sup>.

peak near 0.90 V, a large reduction current peak around 0.81 V, and a broad oxidation current peak between 0.8 and 0.2 V

appear in the voltammogram. The bipolar shape of the voltammogram in the PGPS arises from the superposition of the oxidation of CO and the reduction of the electrode surface.

As is seen from Figure 4, the adsorption and oxidation of CO on the Au(b) electrode yields features similar to those on an Au(a) electrode. The positive shifts of all current peaks by ca. 50 mV is due to the high resistance of the flame-annealed film as described above. Nevertheless, it is noteworthy that the peak oxidation current density is increased to a certain extent by flame annealing. The peak current densities for oxidation of adsorbed CO and solution CO species on Au film electrodes with different surface structures measured from voltammograms in Figure 4 are compared in Table 1. The data indicate that the electrocatalytic activity of the flame-treated Au film electrode toward CO oxidation is slightly higher than that of the as-evaporated Au film electrode.

**3. SEIRAS Studies of CO Adsorption on Au Film Electrodes with Different Surface Structures.** Previous IRAS studies<sup>4,16–20</sup> reported that the IR bands of CO adsorbed on Au electrodes are very weak in acid solutions. Chang and co-workers reported that no CO bands are detectable on an Au-(111) single-crystal electrode in a CO-saturated 0.1 M HClO<sub>4</sub> solution.<sup>20</sup> Nevertheless, we could observe very strong absorption of CO adsorbed on both polycrystalline Au(a) and (111)-oriented Au(b) electrodes by using SEIRAS. A series of spectra of CO adsorbed on a Au(a) electrode in 0.1 M HClO<sub>4</sub> saturated with CO measured as a function of potential are displayed in Figure 5A as a three-dimensional plot. Two characteristic IR bands are seen on the spectra. The more intense band is located at 2110–2136 cm<sup>-1</sup>, which shifts to higher wavenumbers with the potential at a rate of  $\sim 40$  cm<sup>-1</sup>/V. This band has been observed by IRAS and SERS<sup>15,16,19,20</sup> and assigned to linearly bonded CO species (CO<sub>L</sub>). The peak position is much higher than that observed on transition metals (2080–2050 cm<sup>-1</sup> on Pt, Pd, Rh) and closer to that of free CO (2143 cm<sup>-1</sup>), suggesting a weak adsorption. A weaker band is located at 2020–2045 cm<sup>-1</sup>, which also shift to higher wavenumbers at a rate of  $\sim 50$  cm<sup>-1</sup>/V. We tentatively assign this band to linear CO adsorbed at special sites as will be discussed below and denote it as CO<sub>L</sub>(s). On a highly (111)-oriented Au(b) electrode prepared by flame annealing, an additional band is observed around 1930–1970 cm<sup>-1</sup> as shown in Figure 5B. This third weak band can be attributed to bridge-bonded CO species (CO<sub>B</sub>).<sup>15,20</sup> The width (fwhm) of the CO<sub>L</sub> band was about 23 cm<sup>-1</sup> on the Au(a) surface and about 20 cm<sup>-1</sup> on the Au(b) surface over the potential range examined, suggesting that the surface of the Au-(b) electrode is more homogeneous than that of the Au(a) electrode.

Although the spectral features are nearly the same on the two electrodes except for the absence and presence of the weak CO<sub>B</sub> band, the stability of CO<sub>L</sub> is different on the two electrodes. The peak intensities of the three bands measured from Figure 5 are plotted in Figure 6 as a function of the potential. Here, the intensities for CO<sub>L</sub>(s) and CO<sub>B</sub> are multiplied by a factor of 10 for clarity. On the Au(a) electrode (Figure 6A), the intensity of the CO<sub>L</sub> band increases with an increase of electrode potential, reaches its maximum value at about -0.05 V, and then decreases. The intensity of this band disappears at potentials above 0.40 V. On the Au(b) electrode, the CO<sub>L</sub> band survives up to 0.80 V (Figure 6B). The difference of the potential by 150 mV is much larger than the shift of CV (50 mV; see Figures 1 and 4). Chang et al.<sup>20</sup> have reported that the stability of adsorbed CO greatly depends on the crystallography of the electrode surface, and CO is the most stable on (111) among

**TABLE 1: List of Oxidation Current Densities of Adsorbed and Solution CO Species on Au Film Electrodes with Different Treatments<sup>a</sup>**

	$E^1_P$	$j^1_P$	$E^2_P$	$j^2_P$	$E^3_P$	$j^3_P$	$E^1_N$	$j^1_N$	$E^2_N$	$j^2_N$
as evaporated	0.338	101.9	0.962	84.3	1.118	75.3	0.898	39.3	0.585	21.9
flame-treated	0.410	136.7	1.007	98.3	1.274	102.6	0.943	50.1	0.670	39.3

<sup>a</sup> Note:  $E^k_{P,N}$  and  $j^k_{P,N}$  denote the peak potential (V) and current density ( $\mu\text{A cm}^{-2}$ ) of the  $k$ th current peak, respectively, appearing in the PGPS (P) and NGPS (N).

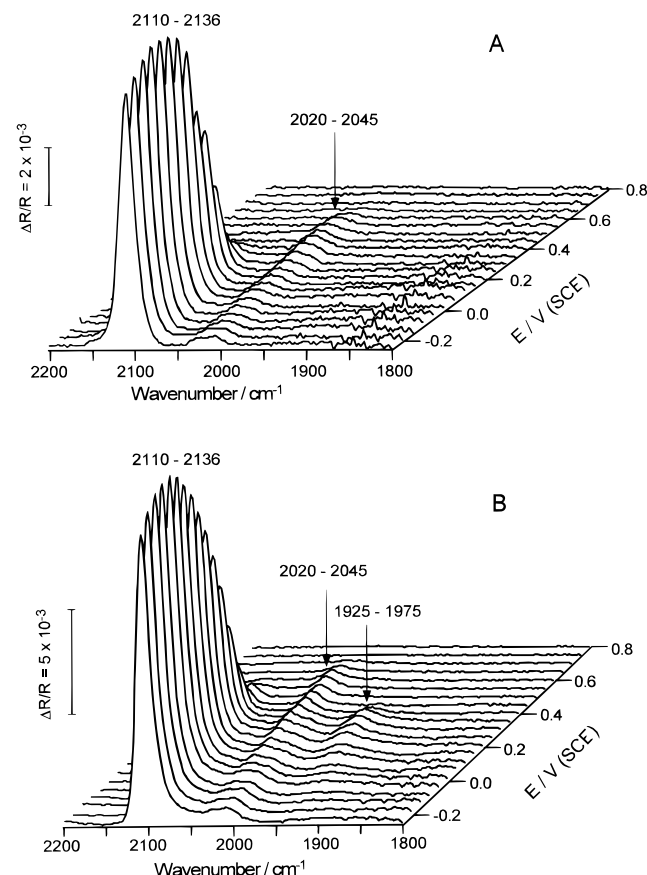


**Figure 5.** A 3-D plot of SEIRA spectra of CO adsorbed from CO-saturated 0.1 M HClO<sub>4</sub> onto an Au film without (A) and with (B) flame annealing acquired as a function of the applied potential.

several single-crystal surfaces they examined. The results obtained in the present study are consistent with those from the former study.

On the other hand, the potential-dependent change in intensity of the CO<sub>L</sub>(s) band is almost the same on the two electrodes: It is almost constant in potential region between -0.20 and 0.20 V, and a maximum appears at around 0.40 V. The band disappears at around 0.65–0.75 V. The higher potential at which the band disappears completely indicates that the CO<sub>L</sub>(s) is adsorbed on the Au surfaces more strongly than CO<sub>L</sub>.

The CO<sub>B</sub> band appears at about 0 V where the CO<sub>L</sub> band starts to decrease and increases in intensity up to 0.3 V associated with the decrease of the CO<sub>L</sub> band. The result suggests that the decrease in surface concentration of CO results in the shift of the adsorption sites from on-top sites to bridge sites. The CO<sub>B</sub> is completely removed from the surface at potentials above 0.45 V by oxidation.

It is interesting and important to compare the band intensities of CO<sub>L</sub> observed by SEIRAS and IRAS. Among CO/metal systems, CO adsorbed on Pt exhibits strongest IR absorption. The peak intensity of CO on Pt electrodes measured in acid solutions by IRAS is  $(2-3) \times 10^{-3}$  in the  $\Delta R/R$  units.<sup>4,5,46,47</sup> The theoretical maximum intensity for a monolayer of CO on

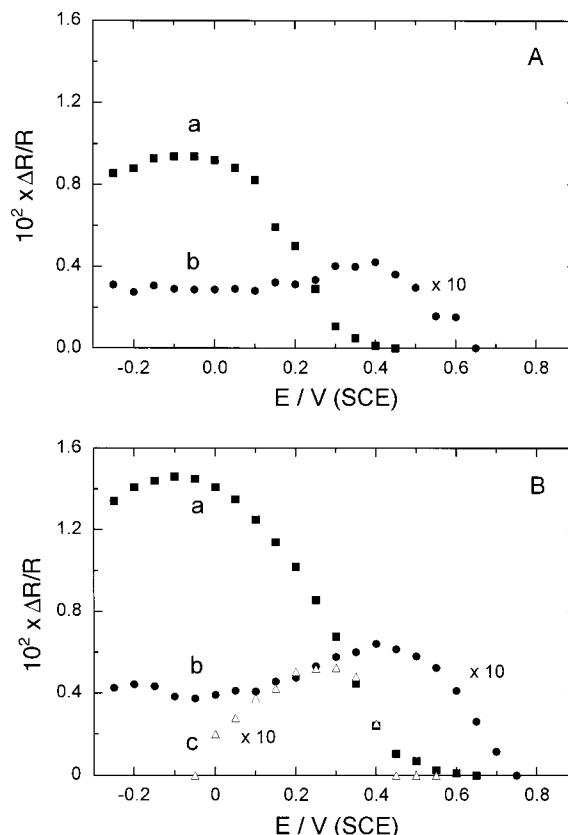


**Figure 6.** Variation of band intensities vs electrode potential for CO species adsorbed on an Au film electrode without (A) and with (B) flame annealing, which are extracted from Figure 5: (a) CO<sub>L</sub> band at 2110–2136 cm<sup>-1</sup>; (b) CO<sub>L</sub>(s) band at 2020–2045 cm<sup>-1</sup>; (c) CO<sub>B</sub> band at 1925–1975 cm<sup>-1</sup>.

Pt surface has been estimated to be ca.  $3 \times 10^{-3}$ .<sup>48</sup> The IR absorption of CO<sub>L</sub> on polycrystalline Au electrodes observed by IRAS is much weaker. The peak intensity observed by Dennis and co-workers<sup>16</sup> in 0.1 M Na<sub>2</sub>SO<sub>4</sub> solution is about  $2 \times 10^{-4}$  (the half value of the peak-to-peak intensity of the bipolar-shaped band). Kumimatsu et al.<sup>18</sup> observed a larger intensity of  $6 \times 10^{-4}$  in 1 M HClO<sub>4</sub>, although the frequency of the CO band they observed (around 2020 cm<sup>-1</sup>) is much lower than that of CO<sub>L</sub> on Au surfaces observed in other IRAS studies.<sup>4,16,19,20</sup> Compared with these values, the maximum peak intensity for CO<sub>L</sub> adsorbed on the Au(a) electrode observed in the present study by SEIRAS is unusually large ( $9.4 \times 10^{-3}$ ; see Figures 5A and 6A), which is much larger than that for CO<sub>L</sub> on Pt. The large surface area of the thin Au film electrode used in the SEIRAS measurements (roughness factor of 3.75) certainly contributes to the large intensity to some extent, but it is too much smaller to explain the extremely large intensity. If the roughness factor of polished polycrystalline Au electrodes used in IRAS measurements is assumed to be 1.65 as for a polished single-crystal Au(111) surface,<sup>49</sup> a 20 times enhancement of IR absorption is calculated compared with the data reported by Dennis and co-workers.<sup>16</sup> The enhancement is more significant for CO<sub>L</sub> adsorbed on the highly ordered (111) Au

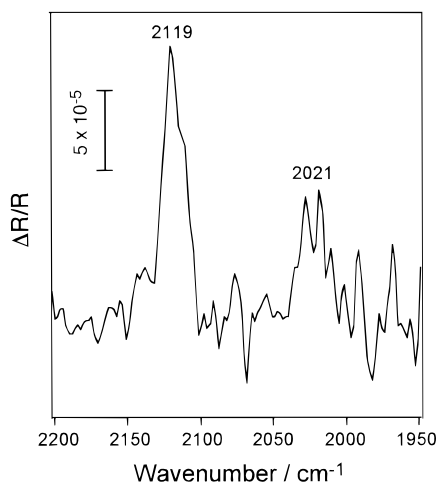


**Figure 7.** SEIRA spectrum showing the effect of removing solution CO species. After the adsorption of CO onto a flame-annealed Au film electrode from CO-saturated  $\text{HClO}_4$  at  $-0.05$  V, CO in the solution was removed by Ar gas bubbling for 10 min and the spectrum was acquired at the same potential.

film electrode prepared by flame annealing. In this case the maximum intensity is  $1.47 \times 10^{-2}$ , from which an enhancement factor of ca. 40 is calculated. The increase in the enhancement factor by flame annealing may be attributed to the change in the shape of metal particles.<sup>28,35</sup>

We observed in Figure 5 a weak IR band at  $2010\text{--}2045\text{ cm}^{-1}$ . From the frequency, this band may be attributed to linearly bonded CO rather than bridge-bonded CO. The high stability of this band shown in Figure 6 indicates that the CO species is adsorbed on the surface more strongly than  $\text{CO}_\text{L}$  species that exhibits the band above  $2100\text{ cm}^{-1}$ . The stronger adsorption is believed to weaken the  $\text{C}\equiv\text{O}$  bond and result in the shift to the lower wavenumber. Thus, we denoted this species as  $\text{CO}_\text{L}(\text{s})$ . However, no such bands have been reported in the most previous IRAS and SERS studies of CO adsorption on Au surfaces in solution<sup>4,15,16,19,20</sup> and in a vacuum.<sup>50</sup> Only Kunimatsu and co-workers<sup>17,18</sup> observed an IR band around  $2020\text{ cm}^{-1}$  on polycrystal Au electrode in 1 M  $\text{HClO}_4$  and assigned this band to  $\text{CO}_\text{L}$ . They reported that this band did not change its intensity when the solution is bubbled with  $\text{N}_2$  gas to remove CO from the solution.

To check whether the  $2010\text{--}2045\text{ cm}^{-1}$  band we observed has the same origin as the  $2020\text{ cm}^{-1}$  band observed by Kunimatsu et al., we compared the spectra acquired before and after removing CO from the solution by Ar gas bubbling. A typical spectrum acquired at  $-0.05$  V after removing CO from the solution is shown in Figure 7. The peak intensities of the  $\text{CO}_\text{L}$  band at  $2119\text{ cm}^{-1}$  and the  $\text{CO}_\text{L}(\text{s})$  band at  $2021\text{ cm}^{-1}$  are  $1.8 \times 10^{-4}$  and  $9 \times 10^{-5}$ , respectively. In comparison with the intensities of  $1.4 \times 10^{-2}$  and  $3.7 \times 10^{-4}$  measured for the two bands in the CO-saturated solution (Figure 5B) collected at the same potential of  $-0.05$  V, it is apparent that both bands are decreased in intensity by removing solution CO. Thus, it is concluded that the CO species observed in the present study is different from that observed by Kunimatsu et al. It is noted that the intensity of the  $\text{CO}_\text{L}$  band is decreased by a factor of about 80, while that of  $\text{CO}_\text{L}(\text{s})$  band is decreased by a factor of only about 4. This result also indicates that the  $\text{CO}_\text{L}(\text{s})$  is adsorbed on the surface more strongly than  $\text{CO}_\text{L}$ .

The  $\text{CO}_\text{L}(\text{s})$  species that yields a band at  $2010\text{--}2045\text{ cm}^{-1}$  are believed to be adsorbed on particular sites existing only on the Au films deposited on a silicon substrate. Molecules are known to be adsorbed at defect sites such as steps and kinks

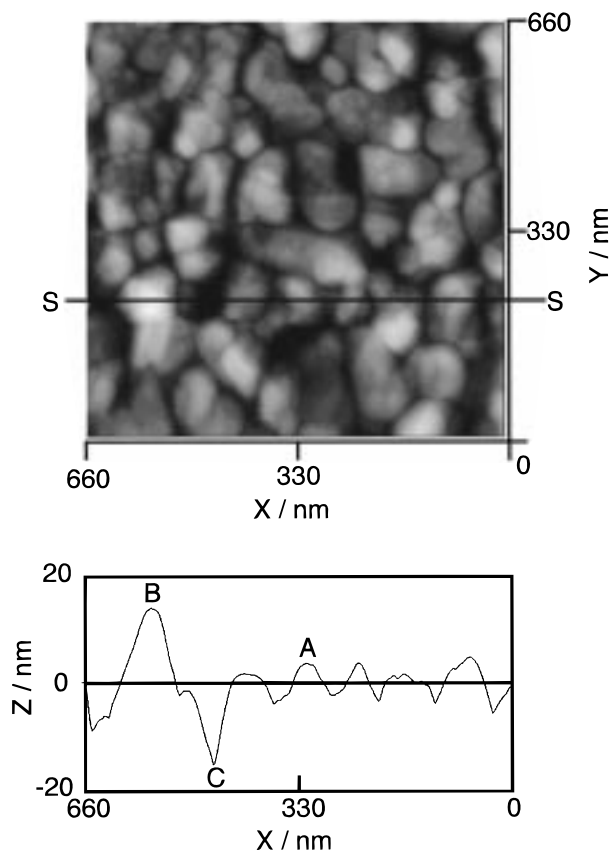


**Figure 8.** STM image of an Au film subjected a potential cycling between  $-0.25$  and  $1.4$  V (upper panel) and a section profile along the S—S line on the image (lower panel).

more strongly than terraces.<sup>51</sup> There exist a number of defect sites on the Au film electrodes as seen from STM images (Figure 3). However, such defect sites are not likely to be the adsorption sites for  $\text{CO}_\text{L}(\text{s})$  because the number of this species is very small. If the absorption coefficients of  $\text{CO}_\text{L}$  and  $\text{CO}_\text{L}(\text{s})$  are assumed to be the same, coverage of  $\text{CO}_\text{L}(\text{s})$  is calculated to be only 3% from the band intensities. It may be worthy to consider the structure of the Au film electrode. As can be seen from the cross section profile of the STM image of an Au(a) film shown in Figure 8, the depth of pore C from the average of the metal surface is about 19 nm, which is very close to the average thickness of 20 nm of the Au film measured by a quartz crystal microbalance. This result suggests that position C is very close to the surface of the silicon substrate. It is known that a very thin silicide (Au—Si alloy) layer is formed when a gold film is grown on silicon.<sup>52,53</sup> Thus, the surface sites indicated by C in Figure 8 is believed to possess a different chemical nature from the top surface of the Au film. We speculate that pores within the Au films are adsorption sites for  $\text{CO}_\text{L}(\text{s})$  rather than the top surfaces of metal particles (A and B).

## Conclusion and Remarks

Thin Au films deposited on silicon were characterized by surface-enhanced IR absorption spectroscopy (SEIRAS), STM, and cyclic voltammetry (CV) by using CO as a probe. STM revealed that 20 nm thick Au films consist of island crystallites with an average size of ca. 60 nm. Voltammetric behavior of the films was identical to that of bulk polycrystalline Au electrodes. It was found by STM and CV that the surface of the gold films becomes highly ordered to (111) orientation by flame annealing. CV showed that the highly ordered (111)



surface prepared by flame annealing has a higher catalytic activity toward CO oxidation than polycrystalline surfaces without flame annealing. Infrared measurements with the Kretschmann configuration revealed that the IR absorption of CO adsorbed on the thin Au film electrodes is significantly enhanced. In comparison with the intensity of CO adsorbed on bulk Au electrodes observed by IRAS, the enhancement factor was estimated to be 20 for as-deposited films and 40 for flame annealed films.

Two linearly bonded CO species,  $\text{CO}_\text{L}$  and  $\text{CO}_\text{L}(\text{s})$ , were identified on the Au thin film electrodes by SEIRAS. The  $\text{CO}_\text{L}$  is predominant on the surface and gives a strong band at 2110–2136  $\text{cm}^{-1}$ , which is close to the vibrational frequency of free CO (2143  $\text{cm}^{-1}$ ) and indicates a weak adsorption. The  $\text{CO}_\text{L}(\text{s})$  is adsorbed on the surface more strongly than  $\text{CO}_\text{L}$  and gives a weak band at 2020–2045  $\text{cm}^{-1}$ . Specific sites located at boundaries of Au crystallites and very close to the substrate surface are speculated to be the adsorption sites for  $\text{CO}_\text{L}(\text{s})$ . An additional CO band assigned to CO species adsorbed at bridge sites was identified on highly ordered Au(111) surfaces in a narrow potential range. This band increases in intensity as the  $\text{CO}_\text{L}$  band decreases in intensity, suggesting a shift of adsorption sites from on-top sites to bridge sites associated with the decrease in coverage of  $\text{CO}_\text{L}$ .

Since signal-to-noise ratio ( $S/N$ ) of spectra are proportional to the square root of the number of interferograms coadded, the IR absorption enhancement is very preferable to collect a spectrum with a good  $S/N$  very quickly and allows time-resolved measurements of electrode reactions. The present study showed that the island nature of the thin Au films plays an important role in SEIRAS. Defect-free single-crystal electrodes are not used in SEIRAS. Nevertheless, it should be noted that fine Au particles have high catalytic activities for several reactions.<sup>54</sup> Thus, this technique is believed to be very useful for the studies of electrocatalysis.

**Acknowledgment.** This work was supported by Grant-in-Aid for Scientific Research on Priority Area of “Electrochemistry of Ordered Interfaces” (No. 09237101) and of “Near-Field Nano-optics” (No. 09241202), for Scientific Research (B) (No. 08454171), and for COE Research Program from the Ministry of Education, Science, Sports and Culture of Japan. S.-G. Sun also thanks Xiamen University, China, for permission for the current collaborative research.

## References and Notes

- (1) Parsons, R.; Van der Noot, T. *J. Electroanal. Chem.* **1998**, 257, 9.
- (2) Beden, B.; Leger, J.-M.; Lamy, C. In *Modern Aspects of Electrochemistry*; Bookris, J. O'M., Conway, B. E., Eds.; Plenum Press: New York, 1992; Vol. 22, Chapter 2.
- (3) Sun, S.-G. In *Electrocatalysis*; Lipkowski, J., Ross, P. N., Eds.; Wiley-VCH: New York, 1998; Chapter 6.
- (4) Beden, B.; Bewick, A.; Kunitake, M.; Lamy, C. *J. Electroanal. Chem.* **1982**, 142, 345.
- (5) Russell, J.-W.; Severson, M.; Scanlon, K.; Overend, J.; Bewick, A. *J. Phys. Chem.* **1983**, 87, 293.
- (6) Kunitake, M.; Seki, H.; Golden, W. G.; Gordon, J. G., II; Philipott, M. R. *Surf. Sci.* **1985**, 158 (5), 96.
- (7) Kunitake, M. *J. Phys. Chem.* **1984**, 88, 2195.
- (8) Kinomoto, Y.; Watanabe, S.; Tokahashi, M.; Ito, M. *Surf. Sci.* **1991**, 242, 538.
- (9) Sun, S.-G.; Chen, A.-C. *J. Electroanal. Chem.* **1992**, 323, 319.
- (10) Lin, W.-F.; Sun, S.-G. *Electrochim. Acta* **1996**, 41, 803.
- (11) Zou, S.-Z.; Gomez, R.; Weaver, M. J. *Langmuir* **1997**, 13, 6713.
- (12) Gomez, R.; Weaver, M. J. *J. Phys. Chem.* **1998**, 102, 3754.
- (13) Motto, S.; Shibata, M.; Watanabe, M. *J. Electroanal. Chem.* **1980**, 110, 103.
- (14) Kita, H.; Nakajima, H.; Hayashi, K. *J. Electroanal. Chem.* **1985**, 190, 141.
- (15) Tadayyoni, M. A.; Weaver, M. J. *Langmuir* **1986**, 2, 179.
- (16) Dennis, S.; Corrigan, S.; Gao, P.; Leung, L. W. H.; Weaver, M. J. *Langmuir* **1986**, 2, 744.
- (17) Nakajima, H.; Kita, H.; Kunitake, M.; Aramata, A. *J. Electroanal. Chem.* **1986**, 201, 175.
- (18) Kunitake, M.; Aramata, A.; Nakajima, H.; Kita, H. *J. Electroanal. Chem.* **1986**, 207, 293.
- (19) Chang, S.-C.; Hamelin, A.; Weaver, M. J. *Surf. Sci.* **1990**, 239, L543.
- (20) Chang, S. C.; Hamelin, A.; Weaver, M. J. *J. Phys. Chem.* **1991**, 95, 5560.
- (21) Takasu, Y.; Ohashi, N.; Zhang, X.-G.; Murakami, Y.; Minagawa, H.; Sato, S.; Yahikozawa, K. *Electrochim. Acta* **1996**, 41, 25.
- (22) Stimming, U.; Friedrich, K. A. Abstracts of 49th ISE meeting, I-2-14-09, Kitakyushu, September 1998.
- (23) Lu, G.-Q.; Sun, S.-G.; Chen, S.-P.; Li, N.-H.; Yang, Y.-Y.; Tian, Z.-W. In *Electrode Processes*; Wieckowski, A., Itaya, K., Eds.; Electrochemical Society, Inc.: New Jersey, 1996; p 436.
- (24) Kunitake, M.; Batina, N.; Itaya, K. *Langmuir* **1995**, 11, 2337.
- (25) Batina, N.; Kunitake, M.; Itaya, K. *J. Electroanal. Chem.* **1996**, 405, 245.
- (26) Hartstein, A.; Kirtley, J. R.; Tsang, J. C. *Phys. Rev. Lett.* **1980**, 45, 201.
- (27) Matsuda, N.; Yoshi, K.; Ataka, K.; Osawa, M.; Uchida, I. *Chem. Lett.* **1992**, 248, 1385.
- (28) Osawa, M.; Ataka, K.; Yoshii, K.; Nishikawa, Y. *Appl. Spectrosc.* **1993**, 47, 1497.
- (29) Nishikawa, Y.; Fujiwara, K.; Ataka, K.; Osawa, M. *Anal. Chem.* **1993**, 65, 556.
- (30) Osawa, M.; Ikeda, M. *J. Phys. Chem.* **1991**, 95, 9914.
- (31) Osawa, M.; Ataka, K.; Yoshii, K.; Yotsuyanagi, T. *J. Electron Spectrosc. Relat. Phenom.* **1993**, 64/65, 371.
- (32) Ataka, K.; Yotsuyanagi, T.; Osawa, M. *J. Phys. Chem.* **1996**, 100, 10664.
- (33) Osawa, M.; Yoshii, K.; Ataka, K.; Yotsuyanagi, T. *Langmuir* **1994**, 10, 640.
- (34) Osawa, M.; Yoshii, K. *Appl. Spectrosc.* **1997**, 51, 512.
- (35) Osawa, M. *Bull. Chem. Soc. Jpn.* **1997**, 70, 2861.
- (36) Lu, G.-Q.; Sun, S.-G.; Chen, S.-P.; Cai, L.-R. *J. Electroanal. Chem.* **1997**, 421, 19.
- (37) Lu, G.-Q.; Sun, S.-G.; Chen, S.-P.; Cai, L.-R.; Tian, Z.-W. *Chem. J. Chin. Univ.* **1997**, 18, 1491.
- (38) Hamelin, A. *J. Electroanal. Chem.* **1996**, 407, 1.
- (39) Angerstein-Kozłowska, H.; Conway, B. E.; Hamelin, A.; Stoicoviciu, L. *J. Electroanal. Chem.* **1987**, 278, 429.
- (40) Angerstein-Kozłowska, H.; Conway, B. E.; Hamelin, A.; Stoicoviciu, L. *Electrochim. Acta* **1986**, 31, 1051.
- (41) Haiss, W.; Lackey, D.; Sass, J. K.; Bespcke, K. H. *J. Chem. Phys.* **1991**, 95, 2193.
- (42) Batina, N.; Will, T.; Kolb, D. M. *Faraday Discuss.* **1992**, 94, 93.
- (43) Batina, N.; Yamada, T.; Itaya, K. *Langmuir* **1995**, 11, 4568.
- (44) Li, N.-H.; Sun, S.-G.; Chen, S.-P. *J. Electroanal. Chem.* **1997**, 430, 57.
- (45) Sun, S.-G.; Chen, S.-P.; Li, N.-H.; Lu, G.-Q.; Chen, B.-Z.; Xu, F.-C. *J. Colloids Surf. As* **1998**, 134, 205.
- (46) Beden, B.; Lamy, C.; Bewick, A.; Kunitake, M. *J. Electroanal. Chem.* **1981**, 121, 343.
- (47) Beden, B.; Bewick, A.; Lamy, C. *J. Electroanal. Chem.* **1983**, 148, 147.
- (48) Beden, B.; Lamy, C. In *Spectroelectrochemistry: Theory and Practice*; Gale, R. J., Ed.; Plenum Press: New York, 1988; Chapter 5.
- (49) Janek, R. P.; Fawcett, W. R. *Langmuir* **1998**, 14, 3011.
- (50) Ruggiero, C.; Hollins, P. J. *Chem. Soc., Faraday Trans.* **1996**, 92, 4829.
- (51) Lipkowski, J.; Stolberg, L. In *Adsorption of Molecules at Metal Electrodes*; Lipkowski, J., Ross, P. N., Eds.; VCH: New York, 1992; Chapter 4.
- (52) Mathieu, G.; Contini, R.; Layet, J. M.; Mathiez, P.; Giorgio, S. J. *Vac. Sci. Technol. A* **1988**, 6, 2904.
- (53) Vancea, J.; Reiss, G.; Scheneider, F.; Bauer, K.; Hoffmann, H. *Surf. Sci.* **1989**, 218, 108.
- (54) Haruta, M. *Catal. Today* **1997**, 36, 153 and references therein.